$^{16}N(0^-)$ beta decay and weak axial vector meson exchange currents

C. A. Gagliardi,* G. T. Garvey, and J. R. Wrobel
Argonne National Laboratory, Argonne, Illinois 60439

S. J. Freedman†
Stanford University, Stanford, California 94305
and Argonne National Laboratory, Argonne, Illinois 60439

(Received 3 June 1983)

We have measured the branching ratio for beta decay of the $J^\pi=0^-$ state at 120 keV in ^{16}N allowing us to infer a beta decay probability of $\Lambda_\beta=(0.45\pm0.05)$ sec^{-1}, in excellent agreement with recent calculations which include pion exchange corrections to the axial vector time component as an essential feature. When combined with the muon capture rate for the inverse reaction, our result implies $g_p/g_A=11\pm2$.

[RADIOACTIVITY $^{16}N(0^-,120$ keV) beta decay, meson exchange currents, weak axial vector current.]

I. INTRODUCTION

The existence of virtual mesons inside nuclei implies a meson exchange contribution to the nuclear weak and electromagnetic currents. It is important to understand these effects because they are a bridge linking the traditional view of the nucleus as a collection of constituent nucleons and more modern interpretations which include non-nucleonic degrees of freedom. At present, theoretical limitations restrict the scope of these studies to processes dominated by the pion.[1,2] Current algebra and soft pion theorems can be used to obtain the one pion exchange currents, and the long range nature of these currents allows their effects in nuclei to be calculated with a minimum of nuclear structure uncertainties. The best evidence to date for meson exchange currents (MEC's) comes from radiative capture of thermal neutrons on hydrogen[3] and the related process of electrodisintegration[4,5] of the deuteron. Here the electromagnetic $M1$ transition operator is strongly modified by MEC's and the pion dominates. The inclusion of pion exchange currents resolves a long-standing discrepancy between theory and experiment. Evidence for axial vector MEC's is less compelling at present.

Kubodera, Delorme, and Rho[6] (KDR) identify a circumstance in which the contributions of weak axial vector MEC's should be large: Phenomena in which the weak axial vector time component dominates. The KDR argument is based on an order of magnitude comparison of the matrix element arising from the weak axial vector current in the impulse approximation and the matrix element from the leading order axial vector pion exchange correction. The diagrams they consider are shown in Fig. 1. To lowest order, Fig. 1(b) is a consequence of soft pion theorems which predict the axial current as the commutator of the vector current and the pion axial charge opera-

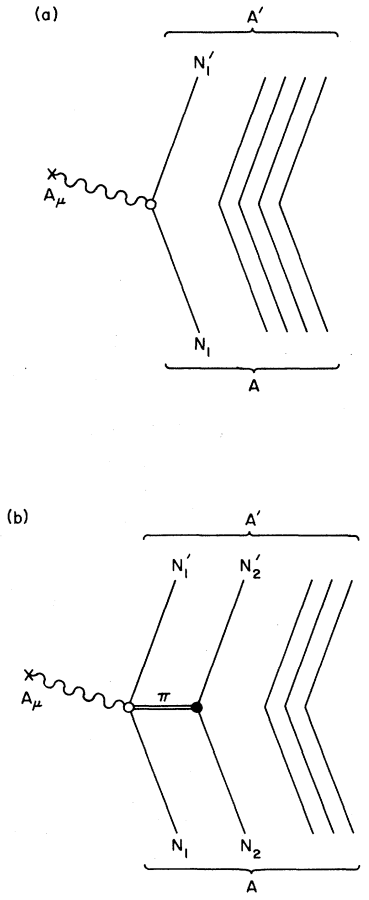

FIG. 1. Diagrams for the nuclear weak axial-vector current (a) in the impluse approximation and (b) with lowest order pion exchange. Open circles represent weak interaction vertices, closed circles are for strong.

tor. Heuristically, the order of magnitude of the one pion exchange correction is given by the A_μ-NNπ vertex where the nucleon part is $\bar{\psi}\gamma_\mu\tau\mp\psi$. Hence, the space component of the vertex correction [Fig. 1(b)] is suppressed to $O(p/m)$, with p and m the nucleon momentum and mass, while the time component is $O(1)$. KDR note that the situation is reversed for axial vector coupling in the impulse approximation, $\bar{\psi}\gamma_\mu\gamma_5\tau\mp\psi$, where the vertex [Fig. 1(a)] is $O(1)$ for the space component and $O(p/m)$ for the time component. The implication is clear: Unraveling one pion exchange corrections in pheneomena where the axial space component dominates (e.g., Gamow-Teller decay rates) is difficult, and the effects from heavier meson exchange and nuclear structure must be well understood. However, in processes that are dominated by the axial time component, pion exchange effects may be easily recognizable corrections to the impulse approximation.

An ideal system for isolating the weak axial charge density is a $0^-\rightarrow 0^+$ beta decay. Here the leading order nonrelativistic matrix elements in the impulse approximation are the axial vector time component, $\langle \vec{\sigma}\cdot\vec{p}/m \rangle$, and the forbidden matrix element, $\langle \vec{\sigma}\cdot\vec{q}\,\vec{r}\rangle$, arising from the space component coupled to one unit of lepton angular momentum. A famous example in light nuclei is the weak decay of the first excited state of ^{16}N,

$$^{16}\mathrm{N}(0^-,120\ \mathrm{keV})\rightarrow {}^{16}\mathrm{O}(0^+,\mathrm{g.s.})+e^-+\bar{\nu}_e\ .$$

This transition has received a great deal of theoretical attention,[6–16] and KDR suggested that MEC corrections to the β-decay rate, Λ_β, may be as large as the impulse approximation predicted rate. Recently, detailed calculations by Towner and Khanna[16] (TK) confirmed this supposition; Λ_β is enhanced by a factor of 3 when MEC's are included. The only previous measurement of the branching ratio for $^{16}\mathrm{N}(0^-)\rightarrow {}^{16}\mathrm{O}(\mathrm{g.s.})$ was reported by the Louvain group,[17,18] who inferred $\Lambda_\beta=0.46\pm0.10\ \mathrm{sec}^{-1}$. The experimental value is consistent with the calculation of TK, suggesting the necessity of MEC's, but the lack of experimental confirmation reduces confidence in the conclusion. Moreover, several authors[9,10,12,13,15,16] have stressed the need for a more precise determination of Λ_β to guide further theoretical work.

The $^{16}\mathrm{N}(0^-)$ beta decay is also interesting as the inverse of the muon-capture reaction:

$$\mu^- + {}^{16}\mathrm{O}(0^+,\mathrm{g.s.})\rightarrow {}^{16}\mathrm{N}(0^-,120\ \mathrm{keV})+\nu_\mu\ .$$

The rate of this muon-capture reaction, Λ_μ, has been considered for many years in attempts to extract the induced pseudoscalar coupling constant, g_p, in finite nuclei. Calculations of Λ_μ depend strongly on the value of g_p, but unfortunately, they also depend upon the details of the particular wave functions used in the calculations. Maksymowicz[19] observes, however, that the ratio $\Lambda_\mu/\Lambda_\beta$ remains sensitive to g_p, but the sensitivity to parameters of the particular model he considers is significantly reduced. More realistic calculations by TK confirm Maksymowicz's result, finding that $\Lambda_\mu/\Lambda_\beta$ is stable to a variety of different residual interactions used to determine the nuclear wave functions. There have been several measurements of Λ_μ; the mean of the most recent two[20,21] gives $\Lambda_\mu=1560\pm94\ \mathrm{sec}^{-1}$. With the calculation of TK and the the Louvain value for Λ_β, the bound for g_p/g_A is $7\leq g_p/g_A\leq 14$. In this analysis the experimental error in Λ_β is a principal limitation.

Given the importance of the $^{16}\mathrm{N}(0^-)$ beta-decay rate and the need for an improved experimental determination, we set out to remeasure the beta-decay branching ratio to higher precision. A preliminary version of the present experiment was previously reported.[22] Since then, a number of changes were made to reduce possible systematic errors, and many more data were obtained. In this paper, we report our final results.

II. EXPERIMENTAL OVERVIEW

Figure 2 shows the various transitions[23] associated with the beta decay of the low-lying levels of ^{16}N. The beta decay of the first excited state competes with $E2$ γ decay to the ground state; consequently the beta branching ratio (R_β) is small ($R_\beta\sim3\times10^{-6}$). Moreover, the signal must be distinguished from a background arising from the decay of the ^{16}N ground state. Since the end point energies differ by only 120 keV out of $\sim$10 MeV, it is impractical to distinguish the β rays from $^{16}\mathrm{N}(0^-)$ decay by their energies. The short lifetime of the 0^- state ($\tau=7.58\pm0.09$ μsec) relative to the ground state ($\tau=10.28\pm0.03$ sec) is the characteristic signature used in the present experiment, as well as in Ref. 17. The experimental approach is directed toward maximizing the "signal" [$^{16}\mathrm{N}(0^-)$ beta decay] relative to the "noise" [^{16}N(g.s.) decay].

^{16}N nuclei in various states of excitation are produced with the $^{15}\mathrm{N}(\mathrm{d,p})^{16}\mathrm{N}$ reaction using ^{15}N-enriched NH_4NO_3 targets and a pulsed 3.8 MeV $^2H_2^+$ beam from the Argonne National Laboratory dynamitron. The $^{16}\mathrm{N}(0^-)$ beta decay branching ratio is determined from simultaneous measurements of β rays with a plastic scintillator telescope and 120 keV deexcitation γ rays with an intrinsic germanium detector. The signal of $^{16}\mathrm{N}(0^-)$ decays is discriminated from the background by measuring

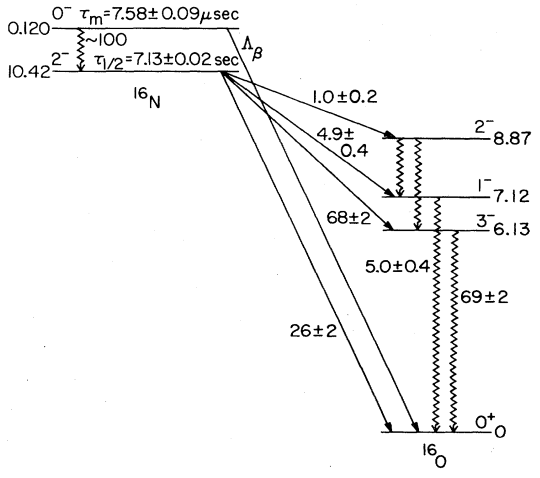

FIG. 2. Transitions of ^{16}N beta decay. Branching ratios in percent include cascading from high levels when appropriate.

the beta decay rate as a function of time relative to the beam pulse and extracting the component with the ≈ 7 μsec lifetime characteristic of ^{16}N(0$^-$) decays.

A multiple target system with a rotating target wheel is employed. Effectively some 782 separate targets are bombarded and counted one after another in a sequence taking about 15 sec to complete. The individual bombardment and counting times, 10 and 63 μsec, respectively, are characteristic of the ^{16}N(0$^-$) lifetime but much shorter than the ^{16}N(g.s.) lifetime. On the other hand, the 15 sec duration of the entire measuring cycle ensures that the ^{16}N produced in each target will be depleted when the cycle is repeated. Thus, the short irradiation and counting periods followed by a long wait period prevent the buildup of ^{16}N(g.s.). The multiple target system is necessary to maintain a favorable duty cycle consistent with the required statistical precision of the measurement. The critical efficiencies of the β detector and γ detector are determined independently.

The germanium γ detector is easily calibrated with sources. The β-detector telescope calibration procedure is less direct. The ^{16}N(g.s.)$\rightarrow$^{16}O(g.s.) decay, which has a β spectrum nearly identical to ^{16}O(0$^-$)$\rightarrow$^{16}O(g.s.) decay, is exploited for one step of the procedure. The β detector is calibrated with the target wheel stopped while the decay rate is monitored with a NaI crystal detecting 6.13 MeV γ decays of the ^{16}O(3$^-$) level. The NaI detector efficiency is measured at 6.13 MeV using the ^{19}F(p,α)^{16}O(3$^-$) resonance reaction and a silicon surface barrier α detector whose efficiency is determined with a calibrated α source. Thus, the calibration is transferred using nuclear reactions from a calibrated α source, to an α detector, to a NaI γ detector, and finally to the β detector used in the experiment. As described in the Appendix, it was necessary to remeasure properties of the ^{19}F(p,α)^{16}O(3$^-$) reaction in a separate experiment in order to expedite the calibration procedure. The error in the known branching ratio for ^{16}N(g.s.)$\rightarrow$^{16}O(3$^-$) relative to ^{16}N(g.s.)$\rightarrow$^{16}O(g.s.) is the limiting factor in the calibration procedure, and ultimately in the final experimental determination of R_β. In the remaining sections we describe some important aspects of the experiment in detail. Further details may be found in Ref. 24.

III. EXPERIMENTAL APPARATUS

Figure 3 is a schematic of the experimental apparatus. The target wheel is an aluminum disk of 50-cm diam and 0.32-cm thick with ten concentric grooves 0.64 cm wide by 0.16 cm deep cut into one surface. The groove diameters range from 26 to 49 cm and the bottom of each is knurled to enhance adhesion of the target material. A concentrated aqueous solution of NH_4NO_3 is distributed in the grooves and allowed to dry in air. The result is a uniform layer of small crystals with an average thickness of about 15 mg/cm^2. Eight grooves contain NH_4NO_3 enriched to 99% ^{15}N, while the second smallest and second largest contain ordinary NH_4NO_3 for background studies.

A motor rotates the target wheel in a vacuum at 3 Hz. The motor is mounted at atmospheric pressure in a housing and connected to the target wheel through a rotating vacuum feed through. The motor housing and target wheel are supported on linear bearings that move on rods as shown in Fig. 3. A screw drive assembly and a precision stepping motor control the target groove position relative to the beam.

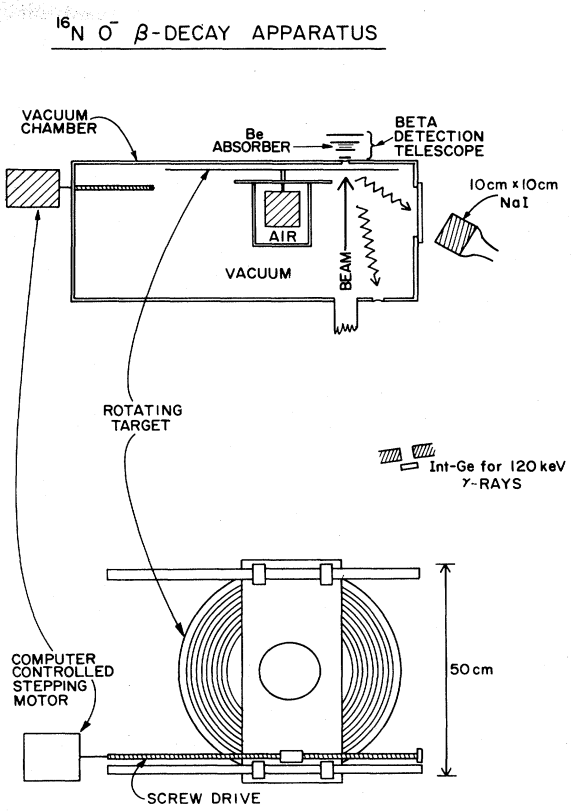

FIG. 3. Diagram of the apparatus.

The 3.8 MeV $^2H_2^+$ beam from the dynamitron is pulsed by two electrostatic deflectors, one horizontal, one vertical, driven by a single high voltage supply. The deflected beam stops in a well-shielded area inside the accelerator vault. Each deflector reduces the beam on target by about 3×10^{-6}, and their combined suppression is $<6\times10^{-8}$. The background, due to beam leakage, is insignificant. The typical instantaneous beam on target is ≈ 30 μA and the deflection system switches the beam in <400 nsec.

An LSI-11/II microcomputer controls and sequences the experiment. The computer controls the frequency of beam pulses and movements of the target wheel so that the target spot being irradiated is separated by at least 1.2 cm from previously irradiated spots. Two microseconds after the irradiation a 63 μsec counting period begins. Movement of the target wheel during irradiation and count periods has a negligible effect on the β- and γ-detector efficiencies.

IV. β-DETECTOR TELESCOPE

Figure 4 depicts the β-detector geometry. Each of the four component counters consists of a thin (≈ 1 mm thick) scintillator coupled through a Lucite light guide to

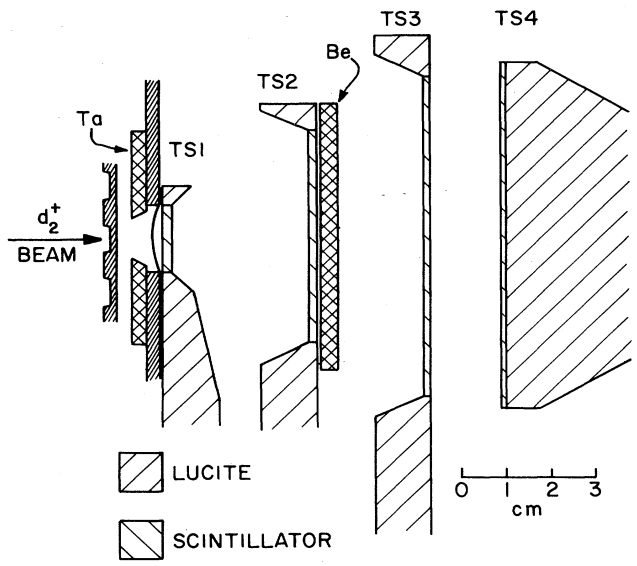

FIG. 4. Schematic diagram of the beta detector telescope. The scintillator thicknesses vary: TS1, 0.16 cm; TS2, 0.16 cm; TS3, 0.11 cm; and TS4, 0.08 cm.

an Amperex XP 2230 photomultiplier.

A tantalum collimator limits the field of view of the telescope, ensuring that the telescope sees only the most recently irradiated target spot. The collimator along with counters TS1 and TS4 (see Fig. 4) restricts the envelope of electron trajectories from the target spot that intersect all four counters, thus defining the effective solid angle, $\Omega \approx 0.58$ sr.

The discriminated signals from the four component counters are required to be in fourfold coincidence with 10 nsec resolving time. The accidental coincidence rate is negligible. Thresholds are set well below the minimum ionization level, making the system insensitive to gain shifts. Typical pulse height spectra from the telescope dectectors are shown in Fig. 5.

A 0.57-cm thick beryllium absorber between detectors TS2 and TS3 prevents β rays from the ^{16}N(g.s.)$\rightarrow ^{16}$O(3^-) transition from triggering the telescope. Insensitivity to β decays to excited states in ^{16}O facilitates one step in the calibration procedure which uses electrons from ^{16}N(g.s.) decay. The absorber also eliminates the possibiilty of confusing electrons from the allowed decay ^{16}N(0^-) $\rightarrow ^{16}$O(1^-,7.12 MeV) with those from the $0^-\rightarrow 0^+$ decay. Finally, the signal to noise in the telescope is enhanced since the absorber reduces the low energy β rays from ^{16}N(g.s.) decay, where only 26% of the transitions go to ^{16}O(g.s.).

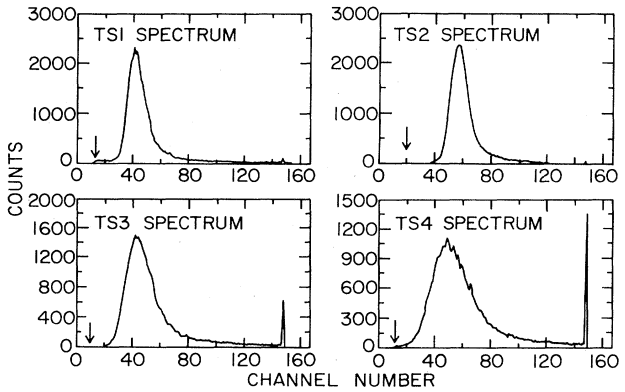

FIG. 5. Telescope pulse height spectra from ^{16}N decay. The arrows indicate the discriminator thresholds. A peak in channel 146 is from ADC overflows.

V. DETECTOR CALIBRATIONS

The 120 keV γ rays are detected in a planar intrinsic Ge detector of 3.8-cm diam by 1.1-cm thick. The Ge detector views the target from 150 cm away through a 1 cm aperture in a lead collimator. The efficiency at 122 keV is measured with a calibrated ^{57}Co source positioned at the target location. The dependence of the efficiency with energy is fit with the lines from a ^{75}Se source and a 1.8% correction gives the efficiency, $(1.88\pm0.03)\times10^{-6}$, at 120 keV.

The β-detector efficiency for the ^{16}N(0^-)$\rightarrow ^{16}$O(g.s.) transition is inferred from measurements of ^{16}N(g.s.) decays. Here we exploit the near equality of the end point energies, and only a small correction to account for the difference in spectral shapes is necessary to relate the two efficiencies.

Calibrations are performed periodically during runs, with the target wheel at rest. The target is irradiated for 7 sec. After a 1 sec "wait" period, ^{16}N(g.s.) decays are counted for 9 sec. The cycle is repeated after a 3 sec wait.

An uncollimated 10-cm diam by 10-cm thick NaI detector 45 cm from the target (see Fig. 3) counts 6.13 MeV γ rays from ^{16}O(3^-,6.13 MeV) decay. The telescope efficiency for the ^{16}N(g.s.)$\rightarrow ^{16}$O(g.s.) transition is given, in the obvious notation, by the expression

$$\epsilon_\beta(2^-\rightarrow 0^+)=\left[\frac{N_\beta}{N_\gamma}\right]\epsilon_\gamma(6.13\text{ MeV})\times\left[\frac{\text{BR}(2^-\rightarrow 6.13\text{ MeV }\gamma\text{ ray})}{\text{BR}(2^-\rightarrow 0^+)}\right].$$

To account for variations in the distance from the target to the beta-detector telescope across the target wheel (estimated at <0.05 cm), calibrations are made for 12 different points on the wheel. The efficiency and its error are taken from the centroid and width of the distribution of measurements.

The NaI detector efficiency, ϵ_γ(6.13 MeV), is determined from separate calibration measurements using the ^{19}F(p,α)^{16}O reaction at the $E_p=340$ keV resonance. Figure 6 is a level diagram showing the important properties of the reaction. For NaI detector calibrations the target wheel is replaced by a single 10 μg/cm^2 MgF_2 target backed with a 15 μg/cm^2 carbon foil. Care is taken to reproduce the source position of the experiment. A 300 mm^2, 100-μm thick partially depleted silicon detector with a Ta collimator is mounted in the target chamber to monitor the ^{19}F(p,α)^{16}O(6.13 MeV) reaction. The Si

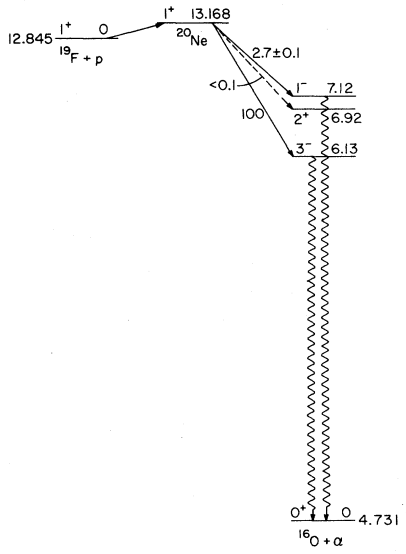

FIG. 6. Transitions following the p+^{19}F capture reaction at $E_p=340$ keV used for calibration. Energy levels are from Ref. 25 and relative branching ratios are from the present work (see the Appendix).

detector efficiency, ϵ_α, is determined to 1% with a calibrated ^{241}Am source. Transitions to ^{16}O(6.13 MeV) are easily resolved in the Si detector. The NaI efficiency is given by

$$\epsilon_\gamma(6.13\ \text{MeV})=\frac{N_\gamma}{N_\alpha}\epsilon_\alpha F_\alpha(\theta_\alpha)F_\gamma(\theta_\gamma)\ ,$$

where θ_α and θ_γ are the angles of the detectors with respect to the beam, and $F_\alpha(\theta_\alpha)$ and $F_\gamma(\theta_\gamma)$ account for the angular distribution of the α and γ rays in the laboratory. These distributions are found to be isotropic in the center of mass in a separate measurement (see the Appendix).

Figure 7 is a typical NaI-detector energy spectrum from the ^{19}F(p,α)^{16}O reaction. The photopeak and escape peaks from 6.13 MeV γ rays are prominent. The arrows indicate the limits used to determine the yield. To account for possible gain shifts, the centroid of the photopeak is used to recalculate the limits of integration for a second integration of the yield determination. Figure 8 is the corresponding spectrum from ^{16}N(g.s.) decay. The difference in the 7.12 MeV γ-ray yields is apparent when Figs. 7 and 8 are compared. The second escape peak and part of the Compton tail of the 7.12 MeV line fall in the region of the 6.13 MeV line, requiring a correction in the efficiency determination. The correction is estimated by assuming the response shape for the 7.12 MeV γ ray is the same as for the 6.13 MeV γ ray. A 20% uncertainty in the correction is assigned to this assumption.

The β detector is slightly sensitive to energetic γ rays which Compton scatter or pair produce (mostly in the Ta collimator). The sensitivity to 6.13 MeV and 7.12 MeV γ rays is measured with a CaF_2 target on 0.16-cm thick aluminum backing, to reproduce the backing of the enriched NH_4NO_3 target. The rate in the β detector is measured at the $E_p=340$ keV resonance with the NaI detector monitoring the reaction rate. The correction for gamma ray sensitivity to the β-detector efficiency is about 6%.

Finally, to get the efficiency for ^{16}N(0$^-$)$\rightarrow$^{16}O(g.s.) decays from the β-detector efficiency for ^{16}N(g.s.)$\rightarrow$^{16}O(g.s.) decays we must correct for the difference in the β spectra. The effective threshold energy of the telescope is inferred from measurements of the telescope efficiency for ^{16}N(g.s.) decays versus beryllium absorber thickness, the theoretical β shapes, and a simple model of multiple scattering. Given the effective threshold, the efficiency correction is obtained by comparing the integrals of the theoretical shapes for the ^{16}N(g.s.)$\rightarrow$^{16}O(g.s.) and the ^{16}N(0$^-$)$\rightarrow$^{16}O(g.s.) transitions. The efficiency $\epsilon_\beta(2^-\rightarrow0^+)$ is multiplied by the factor (1.005±0.011) to give $\epsilon_\beta(0^-\rightarrow0^+)$.

Data taking is divided into three periods, each about 18 h long, with calibrations at the beginning and end of each period. The overall calibrations show a slight nonstatistical deviation, and the β-detector efficiency for each period is obtained from the average of the two associated calibrations with an assigned error large enough to encompass the two.

A typical calibration yields $\epsilon_\beta(0^-\rightarrow0^+)=(1.34$

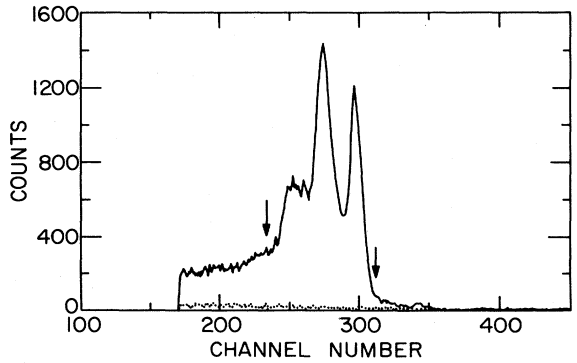

FIG. 7. A NaI pulse height spectrum from p+^{19}F capture at $E_p=340$ keV. The dotted curve is the background spectrum obtained with the beam stopped on a tantalum plate 35 cm from the target.

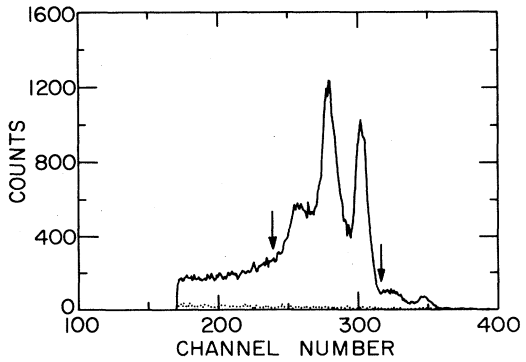

FIG. 8. A NaI spectrum from ^{16}N(g.s.) decay. The dotted curve is the background spectrum obtained with the beam stopped on a tantalum plate.

$\pm 0.15)\times 10^{-2}$. The uncertainty from ^{16}N(g.s.) decay branching ratios, which enter in the ratio

$$\mathrm{BR}(2^- \rightarrow 6.13\ \mathrm{MeV}\ \gamma\ \mathrm{ray})/\mathrm{BR}(2^- \rightarrow 0^+) = \frac{(69\pm 2)\%}{(26\pm 2)\%} ,$$

dominates the experimental error. Reference 26 indicates that these 2% uncertainties are correlated, and thus the uncertainty in the ratio is 11%, a 0.14×10^{-2} contribution to the calibration uncertainty. The uncertainty from all other aspects of the calibration is only 0.04×10^{-2}.

VI. DATA ACQUISITION

To implement "multiscaling" of the γ-detector and β-detector signal rates we measure the time of detection relative to the beam burst with time-to-amplitude converters (TAC's). The common start of each TAC is the beam pulse on target and the stops are hit signals from the detectors. Detector discriminators are gated off while the beam is on target and for an additional 2 μsec "wait" period. The two TAC's are carefully cross calibrated to ensure that β- and γ-ray count rates are measured in the same intervals after the beam burst.

Data are recorded with a PDP 11/45 minicomputer through a CAMAC interface. The important information is the two TAC signals and the energy signal from the Ge detector. In addition, we record the energy signals and timing signals (using a CAMAC time digitizer) from the four counters in the β telescope for studies of systematic errors. Dead times are monitored by comparing the recorded counts in 50 MHz scalers and in the computer. The final results are obtained from an off-line analysis of the individual events recorded on magnetic tape during the experiment.

VII. DATA ANALYSIS AND RESULTS

Figure 9 is the time spectrum of detected β rays during one of the three 18 h run periods. The time spectrum is well represented by an exponential decay with a constant background, the χ^2 per degree of freedom for the fit being 0.75. The measured lifetime is 7.8 ± 0.7 μsec, in good agreement with the accepted value for ^{16}N(0^-). The time spectrum obtained with natural NH_4NO_3 targets is flat and only 5% as large as the constant background with enriched targets. Except for this small constant background, most likely due to neutron capture γ rays, the time spectrum obtained with enriched targets is entirely attributable to ^{16}N decay.

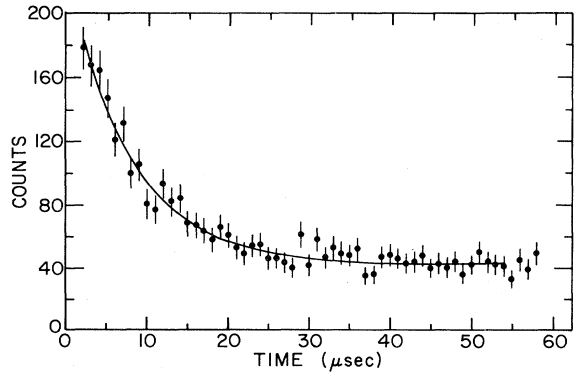

FIG. 9. The β-decay rate as a function of time for an 18 h run. The smooth curve is a fit to an exponential plus a constant.

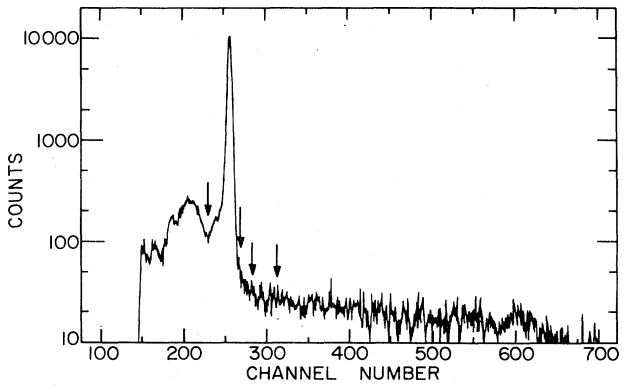

FIG. 10. Intrinsic Ge detector spectrum in the region of the 120 keV γ ray. The arrows indicate the integration region around the peak and an equal sized region for background subtraction.

A Ge-detector energy spectrum from an 18 h run is shown in Fig. 10. Figure 11 is the time spectrum of detected 120-keV γ rays. The window on 120-keV γ rays is identified with arrows in Fig. 10. The second region above 120 keV is used for background subtraction. The resulting time spectrum shown in Fig. 11 is also corrected by 1.5% for dead time losses. The data fit an exponential plus constant, giving 0.8 for the reduced χ^2 per degree of freedom. The lifetime is again consistent and we obtain 7.64 ± 0.10 μsec.

The time dependent populations of ^{16}N(0^-) and ^{16}N(g.s.) after bombardment, denoted $N_0(t)$ and $N_g(t)$, are given by two coupled equations

$$\frac{dN_0}{dt} = -\Lambda_0 N_0 ,$$

$$\frac{dN_g}{dt} = -\Lambda_g N_g + b_\gamma \Lambda_0 N_0 ,$$

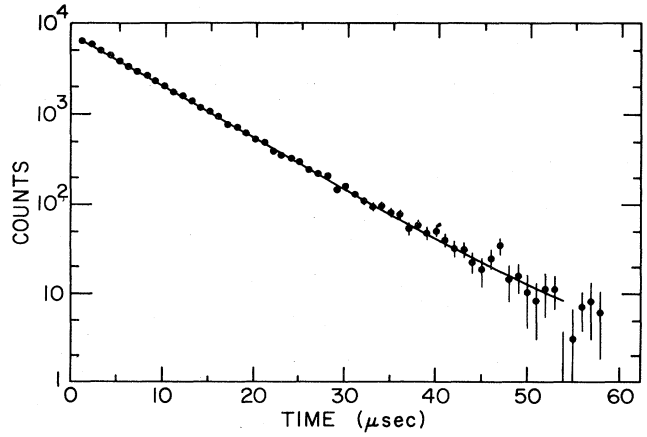

FIG. 11. The background subtracted 120-keV γ-ray rate as a function of time after the beam burst. The curve is a fit to an exponential plus a constant.

where the Λ's are the decay probabilities and b_γ is the γ-decay branching ratio of ^{16}N(0$^-$). We have

$$N_0(t)=N_0(0)e^{-\Lambda_0 t}$$

and

$$N_g(t)=\left[\frac{N_g(0)(\Lambda_g-\Lambda_0)-b_\gamma N_0(0)\Lambda_0}{(\Lambda_g-\Lambda_0)}\right]\times e^{-\Lambda_g t}+\frac{b_\gamma N_0(0)\Lambda_0}{(\Lambda_g-\Lambda_0)}e^{-\Lambda_0 t}\,.$$

To analyze the experiment we may use the following approximations: Λ_g is negligible compared to Λ_0, $\Lambda_g t\approx 0$, and $b_\gamma\approx 1$. We have

$$N_g(t)=N_g(0)+N_0(0)(1-e^{-\Lambda_0 t})\,,$$

and $N_0(t)$ as before. It is important to note that ^{16}N(g.s.) decays produce a time dependent background with the same lifetime as ^{16}N(0$^-$) decay. It is easy to obtain expressions for the β- and γ-detector count rates after the beam burst [recall $R_\beta=\mathrm{BR}(0^-\to 0^+)$]:

$$r_\beta(t)=[\Lambda_0\epsilon_\beta(0^-\to 0^+)R_\beta-\Lambda_g\epsilon_\beta(2^-\to 0^+)\mathrm{BR}(2^-\to 0^+)]N_0(0)e^{-\Lambda_0 t}+\Lambda_g[N_g(0)+N_0(0)]\epsilon_\beta(2^-\to 0^+)$$

and

$$r_\gamma(t)=\epsilon_\gamma(120\text{ keV})\Lambda_0 N_0 e^{-\Lambda_0 t}\,.$$

If we let N_β and N_γ be the yield obtained from fits to the two time spectra, we have

$$R_\beta=\frac{N_\beta}{N_\gamma}\frac{\epsilon_\gamma(120\text{ keV})}{\epsilon_\beta(0^-\to 0^+)}+\Delta R_\beta\,,$$

TABLE I. Sources of experimental uncertainty for the preliminary experiment (Ref. 22) and the present work. All contributions are percent contributions to the ^{16}N(0$^-$) β-decay branching ratio, before the term ΔR_β described in the text is added.

Source	Percent contribution to error: Ref. 22	Present work
Intrinsic-Ge detector calibration[a]		
^{57}Co source calibration accuracy	1.9	1.5
Statistics	2.1	0.8
Variation between 122 and 120 keV	0.5	0.6
Si-detector calibration		
^{241}Am source calibration accuracy	1.0	0.5
Statistics	1.2	0.6
Beam-centroid position uncertainty	1.7	0.5
NaI-detector calibration		
Statistics	1.8	1.1
Target position uncertainty	0.6	0.6
Angular-distribution factor	0.4	0.2
7.12-MeV γ-ray tail correction	0.3	0.3
Beta-detector-telescope calibration		
Statistics	1.2	0.8
7.12-MeV γ-ray tail correction	0.7	0.9
Variation between measurements	3.3[b]	1.5
Telescope sensitivity to ^{16}N(2$^-$) decays to high-lying ^{16}O states	2.6	0.8
0$^-$ and 2$^-$ shape and end point differences	2.0	1.0
^{16}N(0$^-$) branching ratios	10.6	10.6
^{16}N(0$^-$) beta-decay measurement		
Beta-decay yield from time fits	6.7	3.2
Gamma-decay yield from time fits	3.2	0.4
Relative time calibrations	1.0	0.7
Total		
Subtotal, not including ^{16}N(2$^-$) branching ratios	10.2	4.8

[a]A Ge(Li) detector was used during the preliminary measurement.
[b]Only one calibration series was performed. This represents the efficiency variation among the different target locations that were measured.

where

$$\Delta R_\beta = \frac{\Lambda_g}{\Lambda_0} \frac{\epsilon_\beta(2^- \rightarrow 0^+) \mathrm{BR}(2^- \rightarrow 0^+)}{\epsilon_\beta(0^- \rightarrow 0^+)}$$

$$= (0.19 \pm 0.02) \times 10^{-6}$$

is a correction accounting for the buildup of the ^{16}N(g.s.) arising from the γ decay of ^{16}N(0^-).

The final result is obtained from the mean of three separate measurements. We obtain $R_\beta = (3.50 \pm 0.38) \times 10^{-6}$, where 0.35×10^{-6} of the error comes from the uncertainty in ^{16}N(g.s.) decay branching ratios and 0.16×10^{-6} is from all other sources. Table I details the sources of experimental errors in the present measurement as well as in our previous measurement. The agreement between the two experiments is excellent, and so is the agreement with the Louvain result.

Combining our two experimental results with care to account for the common uncertainty of the branching ratios, we have $R_\beta = (3.42 \pm 0.37) \times 10^{-6}$. From the known lifetime we obtain $\Lambda_\beta = 0.45 \pm 0.05$ sec^{-1}. This result is a factor of 2 more precise than the Louvain result. The ^{16}N(g.s.) branching ratio uncertainties are also a source of error in the Louvain measurement, but in that case they are only a small part of the overall error. Thus, this work actually represents a reduction of independent experimental uncertainties by a factor of 5, and it supersedes previous measurements.

A new measurement of the ^{16}N(g.s.) branching ratios intended to reduce uncertainties by a factor of 2 to 3 is underway.[27] When this experiment is completed the experimental error in Λ_β should match the 6% uncertainty in Λ_μ.

VIII. CONCLUSIONS

In Fig. 12 the calculations of Towner and Khanna[16] are displayed as graphs of Λ_μ vs Λ_β for various values of g_p/g_A. Calculations which neglect meson exchange corrections are incapable of giving the experimental values for Λ_μ and Λ_β for any reasonable value of g_p/g_A.

Direct calculations of Λ_μ and Λ_β are sensitive to nuclear wave functions. The TK calculations for different residual interactions give variations of a factor of 6 for Λ_μ and 4 for Λ_β. Despite the remaining uncertainties associated with nuclear wave functions, ^{16}N(0^-) decay provides some of the strongest evidence available for the necessity of MEC contributions to weak nuclear decay.

Four other examples in light nuclei have been studied because of their sensitivity to MEC corrections to the weak axial vector time component: $A=12$ analog beta decays,[28–31] ^{11}Be($\frac{1}{2}^+$)$\rightarrow$^{11}B($\frac{1}{2}^-$,2.12 MeV),[32] ^{16}C(0^+) $\rightarrow$^{16}N(0^-),[33] and ^{18}Ne(0^+)$\rightarrow$^{18}F(0^-,1.08 MeV).[34,35] In $A=12$ the nucleons-only impulse approximation[36] must be enhanced by (45 ± 28)% to agree with experiment, where the error reflects both theoretical and experimental uncertainties. This is in good agreement with the 38% enhancement predicted by calculations which include MEC's. Only preliminary calculations[37,38] are available for ^{11}Be and ^{16}C. One calculation[39] for ^{18}Ne which includes multihole components in the wave function indicates the need for MEC effects to enhance the predicted decay rate, but sensitivity to different residual interactions has not been studied.

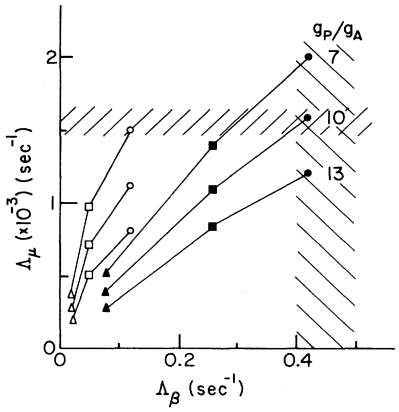

FIG. 12. Calculations of Ref. 16 compared to the experimental values for Λ_μ, from Refs. 20 and 21, and Λ_β, from this work. The open points are impluse approximation calculations and the closed points include MEC's. The circles, boxes, and triangles are from calculations with three different residual interactions. Curves for three values of g_p/g_A are shown. The lines are to guide the eye.

Combining the measured values of Λ_μ and Λ_β with the calculations of TK, we find $g_p/g_A = 11 \pm 2$. This result is model dependent, but in the available calculations the ratio $\Lambda_\mu/\Lambda_\beta$ used to determine g_p/g_A is rather insensitive to the particular model. The other recent determinations of the induced pseudoscalar coupling obtain $g_p/g_A = 7.0 \pm 1.5$, from μ capture on hydrogen,[40] and $g_p/g_A = 9.0 \pm 1.7$, from μ capture on ^{12}C.[41] The ^{12}C result is somewhat model dependent. There is the interesting suggestion from the data that g_p may be enhanced in nuclear matter.

This research was supported by the U.S. Department of Energy under Contract No. W-31-109-Eng-38.

APPENDIX

The procedure of calibrating the NaI detector using the ^{19}F(p,α)^{16}O reaction at the 340 keV proton capture resonance requires a correction for branching ratios and the α- and γ-ray angular distributions. Figure 6 is the relevant level scheme.[25]

For the single reaction channel proceeding through the ^{20}Ne(1^+,13.168 MeV) intermediate state, the α-particle angular distribution in the center of mass can be written in the form[42]

$$W(\Theta_\alpha) = 1 + aP_2(\cos\Theta_\alpha) .$$

The angular distribution coefficient, a, depends on the relative $L=0$ and $L=2$ amplitudes for the incident proton, but not on the particular excited state in ^{16}O. The angular distribution of deexcitation γ rays in ^{16}O has the form[43]

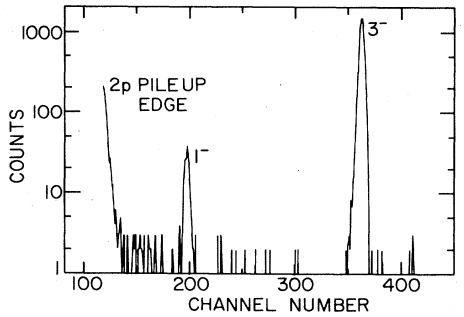

FIG. 13. A typical Si-detector pulse-height spectrum at $\Theta_{lab}=143°$. The α particle lines from ^{19}F(p,α)^{16}O are identified by the J^π of the level in ^{16}O. Proton pileup is the main source of background.

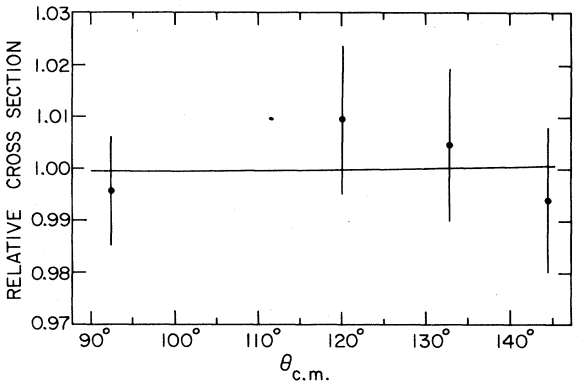

FIG. 14. The measured α-particle angular distribution from ^{19}F(p,α)^{16}O(3$^-$,6.13 MeV) at $E_p=340$ keV. The solid line is a fit with the function $W(\Theta_\alpha)=N\{1+aP_2[\cos(\Theta_\alpha)]\}$.

$$W(\theta_\gamma)=1+a\epsilon_s P_2(\cos\theta_\gamma)\ ,$$

where a is the same as before but ϵ_s is a factor that depends upon the state in ^{16}O. With subscripts indicating spin, we have $\epsilon_3=0.75$, $\epsilon_2=0.50$, and $\epsilon_1=-0.50$. A previous measurement[44] of the alpha-particle angular-distribution coefficient obtained $a=(0.014\pm0.028)$. Meanwhile, tails from the 6.92- and 7.12-MeV γ-ray lines fall under the 6.13 MeV region in the NaI detector calibration spectrum. Thus, the alpha-particle branching ratios must be known to correct the 6.13 MeV γ-ray yield. The only previously meausred branching ratio[45] values have low precision.

We made a study of the 340 keV ^{19}F(p,α)^{16}O resonance to better determine the branching ratios and to reduce the uncertainty in a. An 80-nA, 340-keV proton beam irradiates a 14 μg/cm^2 MgF_2 target evaporated on a 15 μg/cm^2 carbon backing. The target is at 45° to the beam. Three 50 mm^2 silicon detectors 17 cm from the target count α particles. One detector is moved over the range $90°\leq\theta_{lab}\leq143°$ measuring the angular distribution, while the other two are fixed at $\theta_{lab}=-90°$ and $+158°$, serving as monitors.

Figure 13 is a typical spectrum from the movable detector, and Fig. 14 is the measured angular distribution transformed to the center of mass. A fit yields $a=(0.001\pm0.017)$, where the uncertainty is purely statistical. We estimate the systematic uncertainty from possible misalignments and beam shifts to be $\leq0.015\%$. The branching ratio to the ^{16}O(1$^-$,7.12 MeV) state is $(2.7\pm0.1)\%$ of the branch to the 3$^-$ state. We find no evidence for a decay to ^{16}O(2$^+$,6.92 MeV); the branching ratio is $\leq0.1\%$.

*Present address: Cyclotron Institute, Texas A&M University, College Station, TX 77843.

†Present address: Argonne National Laboratory, Argonne IL 60439.

[1]*Mesons in Nuclei,* edited by M. Rho and D. H. Wilkinson (North-Holland, Amsterdam, 1979).

[2]M. Ericson, Prog. Part. Nucl. Phys. 1, 67 (1978).

[3]D. O. Riska and G. E. Brown, Phys. Lett. 38B, 193 (1972).

[4]J. Hockert, D. O. Riska, M. Gari, and A. Huffman, Nucl. Phys. A217, 14 (1973).

[5]M. Bernheim, E. Jans, J. Mougey, D. Royer, D. Tarnowski, S. Turck-Chiez, I. Sick, G. P. Capitani, E. DeSanctis, and S. Frullani, Phys. Rev. Lett. 46, 402 (1981).

[6]K. Kubodera, J. Delorme, and M. Rho, Phys. Rev. Lett. 40, 755 (1978).

[7]A. Bottino, G. Ciocchetti, and C. W. Kim, Phys. Rev. C 16, 1120 (1977).

[8]P. Guichon, M. Giffon, J. Joseph, R. Laverriere, and C. Samour, Z. Phys. A 285, 183 (1978).

[9]P. A. M. Guichon, M. Giffon, and C. Samour, Phys. Lett. 74B, 15 (1978).

[10]P. A. M. Guichon and C. Samour, Phys. Lett. 82B, 28 (1979).

[11]B. R. Holstein and C. W. Kim, Phys. Rev. C 19, 1433 (1979).

[12]K. Koshigiri, H. Ohtsubo, and M. Morita, Prog. Theor. Phys. 62, 706 (1979).

[13]W. K. Cheng, B. Lorazo, and B. Goulard, Phys. Rev. C 21, 374 (1980).

[14]W. K. Cheng and B. Goulard, Phys. Rev. C 23, 869 (1981).

[15]J. Delorme, Nucl. Phys. A374, 541c (1982).

[16]I. S. Towner and F. C. Khanna, Nucl. Phys. A372, 331 (1982).

[17]L. Palffy, J. P. Deutsch, L. Grenacs, J. Lehmann, and M. Steels, Phys. Rev. Lett. 34, 212 (1975).

[18]The value of Λ_β reported in Ref. 17 was obtained neglecting the effect of the buildup of ^{16}N(g.s.) described in the text. [J. P. Deutsch (private communication).]

[19]A. Maksymowicz, Nuovo Cimento A 48, 320 (1967).

[20]F. R. Kane, M. Eckhause, G. H. Miller, B. L. Roberts, M. E. Vislay, and R. E. Welsh, Phys. Lett. 45B, 292 (1973).

[21]P. Guichon, B. Bihoreau, M. Giffon, A. Goncalves, J. Julien, L. Roussel, and C. Samour, Phys. Rev. C 19, 987 (1979).

[22]C. A. Gagliardi, G. T. Garvey, J. R. Wrobel, and S. J. Freedman, Phys. Rev. Lett. 48, 914 (1982).

[23]F. Ajzenberg-Selove, Nucl. Phys. A375, 1 (1982).

[24]C. A. Gagliardi, Ph.D. thesis, Princeton University, 1982 (unpublished).

[25]F. Ajzenberg-Selove, Nucl. Phys. A300, 1 (1978).
[26]D. E. Alburger, A. Gallmann, and D. H. Wilkinson, Phys. Rev. 116, 939 (1959).
[27]A. Heath and G. T. Garvey (unpublished).
[28]P. Lebrun, Ph. Deschepper, L. Grenacs, J. Lehmann, C. Leroy, L. Palffy, A. Possoz, and A. Maio, Phys. Rev. Lett. 40, 302 (1978).
[29]H. Brandle, L. Grenacs, J. Lang, L. Ph. Roesch, V. L. Telegdi, P. Truttmann, A. Weis, and A. Zehnder, Phys. Rev. Lett. 40, 306 (1978).
[30]H. Brandle, G. Miklos, L. Ph. Roesch, V. L. Telegdi, P. Truttmann, A. Zehnder, L. Grenacs, P. Lebrun, and J. Lehmann, Phys. Rev. Lett. 41, 299 (1978).
[31]Y. Masuda, T. Minamisono, Y. Nojiri, and K. Sugimoto, Phys. Rev. Lett. 43, 1083 (1979).
[32]E. K. Warburton, D. E. Alburger, and D. H. Wilkinson, Phys. Rev. C 26, 1186 (1982).
[33]C. A. Gagliardi, G. T. Garvey, N. Jarmie, and R. G. H. Robertson, Phys. Rev. C 27, 1353 (1983).
[34]E. G. Adelberger, C. D. Hoyle, H. E. Swanson, and R. D. Von Lintig, Phys. Rev. Lett. 46, 695 (1981).
[35]A. M. Hernandez and W. W. Daehnick, Phys. Rev. C 25, 2957 (1982).
[36]P. A. M. Guichon and C. Samour, Nucl. Phys. A382, 461 (1982).
[37]D. J. Millener, D. E. Alburger, E. K. Warburton, and D. H. Wilkinson, Phys. Rev. C 26, 1167 (1982).
[38]D. Kurath (private communication).
[39]W. C. Haxton, Phys. Rev. Lett. 46, 698 (1981).
[40]G. Bardin, J. Duclos, A. Magnon, J. Martino, A. Richter, E. Zavattini, A. Bertin, M. Piccinini, and A. Vitale, Phys. Lett. 104B, 320 (1981).
[41]L. Ph. Roesch, V. L. Telegdi, P. Truttmann, A. Zehnder, L. Grenacs, and L. Palffy, Phys. Rev. Lett. 46, 1507 (1981).
[42]J. M. Blatt and L. C. Biedenharn, Rev. Mod. Phys. 24, 258 (1952).
[43]H. J. Rose and D. M. Brink, Rev. Mod. Phys. 39, 306 (1967).
[44]J. A. Van Allen and N. M. Smith, Phys. Rev. 59, 501 (1941).
[45]J. M. Freeman, Philos. Mag. 41, 1225 (1950).